

High-Temperature Behavior of Cellulose I

James F. Matthews,^{*,†} Malin Bergenstråhlé,^{‡,§} Gregg T. Beckham,^{¶,||,¶} Michael E. Himmel,[†] Mark R. Nimlos,[⊥] John W. Brady,[‡] and Michael F. Crowley^{*,†}

[†]Biosciences Center, National Renewable Energy Laboratory, Golden, Colorado, United States

[‡]Department of Food Science, Cornell University, Ithaca, New York, United States

[§]Wallenberg Wood Science Center, Royal Institute of Technology, Stockholm, Sweden

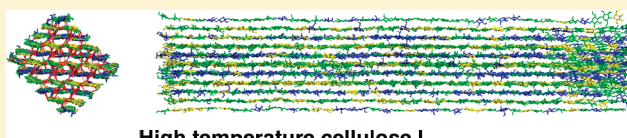
[⊥]National Bioenergy Center, National Renewable Energy Laboratory, Golden, Colorado, United States

^{||}Department of Chemical Engineering, Colorado School of Mines, Golden, Colorado, United States

[¶]Renewable and Sustainable Energy Institute, Boulder, Colorado, United States

 Supporting Information

ABSTRACT: We use molecular simulation to elucidate the structural behavior of small hydrated cellulose I β microfibrils heated to 227 °C (500 K) with two carbohydrate force fields. In contrast to the characteristic two-dimensional hydrogen-bonded layer sheets present in the cellulose I β crystal structure, we show that at high temperature a three-dimensional hydrogen bond network forms, made possible by hydroxymethyl groups changing conformation from trans-gauche (TG) to gauche-gauche (GG) in every second layer corresponding to “center” chains in cellulose I β and from TG to gauche-trans (GT) in the “origin” layer. The presence of a regular three-dimensional hydrogen bond network between neighboring sheets eliminates the possibility of twist, whereas two-dimensional hydrogen bonding allows for microfibril twist to occur. Structural features of this high-temperature phase as determined by molecular simulation may explain several experimental observations for which no detailed structural basis has been offered. This includes an explanation for the observed temperature and crystal size dependence for the extent of hydrogen/deuterium exchange, and diffraction patterns of cellulose at high temperature.



High temperature cellulose I

INTRODUCTION

As the most abundant biological material on Earth, cellulose is a key constituent in the global carbon cycle and is an attractive renewable feedstock for mankind's energy needs. Cellulose is the linear polymer of (1,4) β -D-glucose, and it is known to crystallize into multiple polymorphs with each polymer chain containing up to the order of 10³–10⁴ monomers. The crystalline fraction of native cellulose is a combination of two crystalline polymorph phases termed cellulose I β and cellulose I α , which differ mainly in the pattern of layer stacking from the recently solved crystal structures.^{1–6} Experimental work has shown that thermal treatment can change cellulose structure. For example, Wada and co-workers conducted a series of X-ray diffraction studies on the thermal expansion of lattice spacing in cellulose.^{7–11} These experiments measured lattice parameters and diffraction patterns of cellulose as a function of temperature, showing a discontinuous change in lattice spacing during heating, but the molecular level structure was not elucidated.

Throughout this paper, we will use the term “microfibril” to mean the unit produced by a cellulose synthase terminal complex, which in plants is likely to be a rosette of 36 synthase subunits and which are larger linear complexes in some algae and in bacteria.^{12–15} This terminology follows the same convention as was used in the recent review article by Nishiyama,¹⁶ but

historically distinctions between the terms “elementary fibril”, “microfibril”, and “fibril” have not been consistent.^{17,18} Many experimental studies of cellulose structure use very large diameter (~10–20 nm and larger) microfibrils from algae, bacteria, and tunicates. These crystalline materials do not have quantitatively the same phase behavior and temperature response as the 2–5 nm diameter cellulose microfibrils from plants, due to differences in crystallite diameter.^{19–25} This situation complicates the study of cellulose polymorphs because polymorph stability and thermodynamic barriers to solid–solid phase transformations are a function of crystallite size.^{26–28} It is known that large-diameter cellulose I α microfibrils will transform to cellulose I β through thermal annealing with a minimum required temperature in the range of 260 to 280 °C, depending on the polarity of the surrounding medium,²⁹ but it is unclear whether or not these experiments on large-diameter microfibrils at elevated temperature elucidate the behavior of small-diameter cellulose microfibrils at the same temperature. As thermal and chemical treatment of cellulose is required for utilization of this vast resource for production of renewable fuels and chemicals,³⁰

Received: October 26, 2010

Revised: January 21, 2011

Published: February 22, 2011

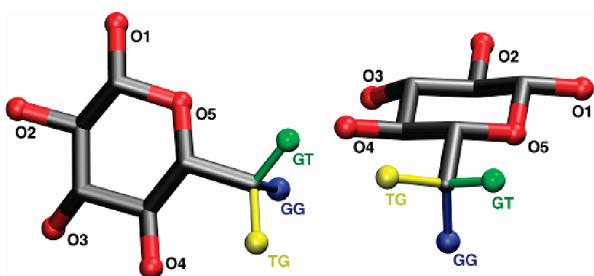


Figure 1. Conformations of the β -D-glucose primary alcohol group. Hydrogen atoms are omitted, and the GT (green), TG (yellow), and GG (blue) labels refer to the gauche or trans position of O6 relative to both O5 and C4.

the behavior of cellulose at high temperature is of significant scientific and industrial relevance.

With knowledge from recent crystal structures solved for natural cellulose^{3–6} and other known cellulose polymorphs,^{5,31,32} it is possible to probe the molecular level behavior of cellulose at high temperature using computational approaches. Here, we apply molecular dynamics (MD) simulations to elucidate the high-temperature behavior of cellulose I β , in an effort to better understand results from the large body of experimental literature that has studied cellulose behavior as a function of temperature.

■ BACKGROUND

Glucose and Cellobiose. As an introduction to cellulose conformation and crystal packing, we briefly review glucose and cellobiose conformation and nomenclature. Glucose is a six-membered ring with four hydroxyl groups and a hydroxymethyl group around the perimeter (Figure 1). Glucose can adopt many ring pucker conformations, but the favored form is the 4C_1 chair, where the hydroxymethyl group is equatorial.³³ The hydroxyl group at C1 can rearrange via ring-opening in a process called mutarotation to become axial or equatorial, with β -glucose having the equatorial configuration and α -glucose having the axial configuration when the ring adopts the usual 4C_1 chair form.³⁴ The open ring aldehyde form of glucose can participate in redox reactions; thus the cellulose chain end with a hydroxyl group at C1 is referred to as the reducing end whereas the chain end with a hydroxyl group at C4 is called the nonreducing end. The hydroxymethyl group at C6 has three low-energy rotameric conformations, which can be given a two-letter name by the two trans or gauche dihedral relationships with first the ring oxygen O5—C5—C6—O6 and second C4—C5—C6—O6. In aqueous solution and in vacuum, the gauche-trans (GT) rotamer is most populated, with GG slightly less populated and TG least populated.^{35–38} The hydroxymethyl group of glucose in water rotates at the nanosecond time scale.³⁹ Figure 1 shows these three rotamers of glucose in the color scheme that will be continued throughout this study with GT colored green, GG colored blue, and TG colored yellow.

Cellobiose is the disaccharide of β (1,4)-linked D-glucose monomers connected via a glycosidic bond, and is the smallest molecule with the same repeating constitutional structure as cellulose. In crystal structures and in solution, cellobiose prefers slightly twisted conformations but crystal packing in the vast majority of cellulose crystals favors a nearly flat 2-fold screw conformation.^{40–44} With this glycosidic linkage conformation, a hydrogen bond from HO3 on the reducing end sugar to the ring

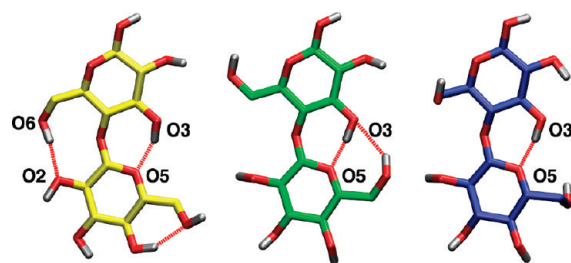


Figure 2. Three cellobiose primary alcohol group conformations, TG/TG, GT/GT, and GG/GG left to right, with hydrogen bonds shown as dashed red lines. The glycosidic linkage conformation is as in cellulose I. Aliphatic hydrogen atoms are omitted. The color scheme for carbon atoms is the same as shown for the primary alcohol group in Figure 1. The reducing end is on top, and the nonreducing end is on bottom.

oxygen O5 on the nonreducing end sugar is possible. Three conformations of cellobiose are shown in Figure 2, with the carbon atoms colored by the primary alcohol conformation as in Figure 1. The TG hydroxymethyl group conformation at the reducing end makes possible a hydrogen bond from the reducing end O6 to the nonreducing end O2. The GT conformation at the reducing end moves O6 too far away from the nonreducing end O2 for this hydrogen bond to form. With the GG conformation at the reducing end, hydrogen bonding between O6 and O2 is possible for certain conformations of the glycosidic linkage.

Cellulose Crystals. Multiple cellulose crystal structures have recently been solved with X-ray and neutron fiber diffraction, including cellulose I β and I α .^{3–6} There are significant similarities between the cellulose I β and I α polymorphs. The cellulose I β and I α structures consist of parallel, two-dimensional hydrogen-bonded sheets with all hydroxymethyl groups in the TG conformation, and the average plane of the glucose rings in the same plane as the hydrogen-bonded sheet. All other crystal structures of cellulose polymorphs, such as cellulose II⁵ and III_L,³¹ have the average glucose ring plane tilted relative to the plane of neighboring cellulose chains. This tilt allows for the presence of hydrogen bonds between neighboring layers, producing a three-dimensional hydrogen bond network. Chain packing, hydrogen bonds, and tilt within cross sections are illustrated in Figure 3 for cellulose I β , I α , II, and III_L.

Polymer Crystal Defects and Twist. Twist in cellulose microfibrils is incompatible with the traditional notion of an ideal crystal, where there is perfect periodicity in three dimensions. Polymer crystals can be defined as polymers with discrete diffraction spots, which allows for the incorporation of a variety of defects.^{45,46} Many experimental observations^{47–50} and simulations^{51–53} of cellulose show twist in cellulose microfibrils can exist. If cellulose chains are fully extended along the length of a microfibril, any twist in the microfibril requires some amount of slip between or within hydrogen-bonded layers. Point defects such as broken chains, which can be characterized with a Burger's vector,⁵⁴ are also likely to exist. A layer slip defect is termed a stack fault, and these types of faults can shift peak locations in diffraction patterns.^{46,55,56} Stack faults explain the observation of cellulose I α and I β coexistence along the length of single microfibrils, as this difference in layer packing is the essential difference between cellulose I α and I β .⁵⁷ The energy required for twisting an inelastic sheet is proportional to the fourth power of the sheet diameter,⁵⁸ meaning twist in cellulose is much more likely to be observed in small-diameter microfibrils than in large-diameter

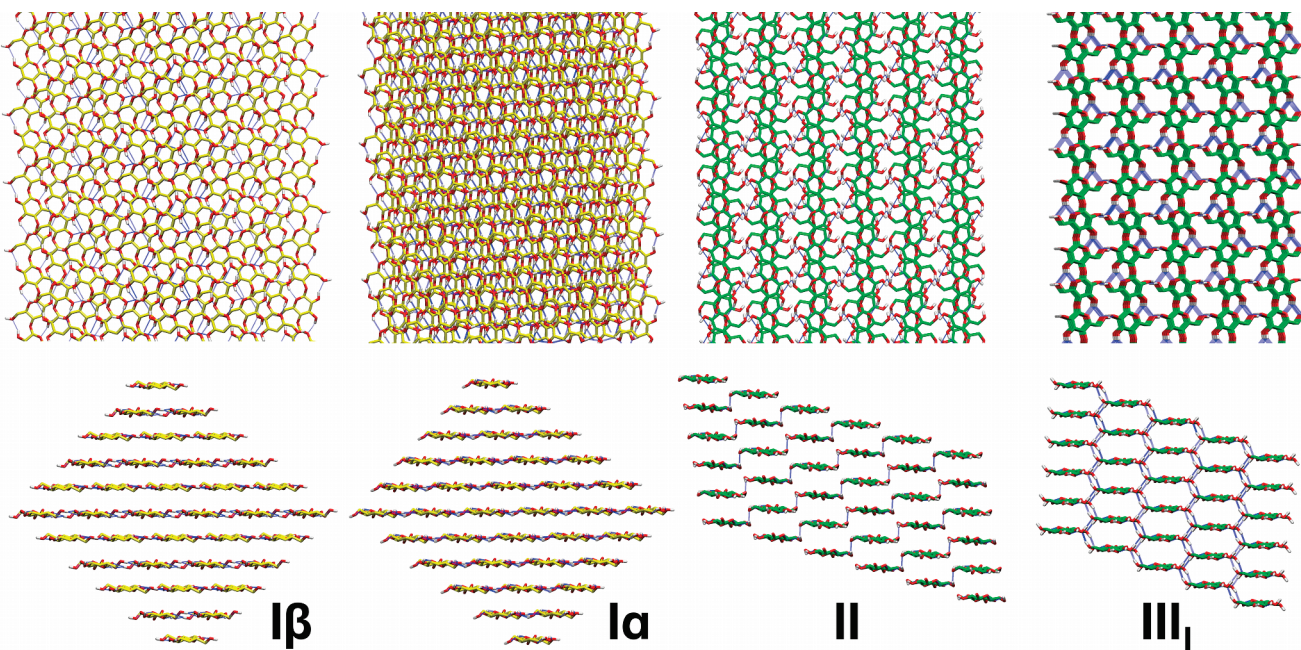


Figure 3. Structures of cellulose I β , I α , II, and IIII illustrating differences in chain tilt, packing and hydrogen bonding.

microfibrils. It is a general result that thin elastic rods made of chiral repeating units can have a helical structure as the free energy minimum;^{59,60} however, the low elasticity of cellulose polymer chains severely limits the amount of twist possible in large-diameter cellulose microfibrils.^{58,61} Kinks with rotating orientation along the microfibril axis (which implies twist) have been observed on the tens of nanometers length scale in tomographic reconstructions of ~ 3 nm diameter wood cellulose microfibrils,⁴⁸ but large ~ 20 nm diameter microfibrils from *Valonia* retain a constant uniplanar alignment relative to the native cell wall surface.⁶² Upon isolation, individual *Valonia* and *Halocynthia* cellulose microfibrils show kinks⁶³ or twist.⁴⁷ Rowland and Roberts in 1972 determined that cotton cellulose also has short segments that are twisted and are accessible to chemical substitution.⁶⁴

High-Temperature Behavior of Cellulose. Experimental studies have examined the behavior of cellulose I β and I α as a function of temperature using multiple experimental techniques. Several diffraction studies demonstrated anisotropic expansion in cellulose crystals, with non-hydrogen-bonded layer lattice spacing expanding more than spacing within a hydrogen-bonded layer.^{7–11} These studies show that the thermal expansion coefficient of cellulose is discontinuous when reaching 250–260 °C, indicating a phase transformation. An unusual property of the reported diffraction patterns at high temperature for cellulose I β is the presence of odd-order diffraction peaks, which should be disallowed for the reported $P2_1$ space group, as Wada and co-workers note.¹¹

Spectroscopy experiments of cellulose show discontinuous behavior as the temperature approaches 180–220 °C.^{65,66} Watanabe and co-workers used 2D moving window infrared (MWIR) spectroscopy to show that there is an abrupt change in hydrogen bond structure in this temperature range. The authors used IR peak assignments of the room temperature molecular conformations proposed by Maréchal and Chanzy;⁶⁷ however, these peak assignments indicate the presence of GG and GT

conformations, which does not agree with the TG primary alcohol conformation of cellulose I α and cellulose I β at room temperature as determined by solid-state NMR and diffraction experiments.

Sugiyama and co-workers showed with IR spectroscopy that the interior of cellulose microfibrils is inaccessible to hydrogen/deuterium (H/D) exchange at room temperature; however, this exchange can proceed to the interior at elevated temperature during 1 h of exchange time.⁶⁸ The increase in layer spacing shown from X-ray diffraction is not sufficient to allow water molecules to permeate between the cellulose chains, and so this difference in accessibility to exchange in the high-temperature phase indicates a significant change in hydrogen bond pattern. Microfibril diameter is correlated with the minimum temperature required to initiate increased layer spacing and to complete H/D exchange, with large (~ 20 nm) diameter microfibrils from algae requiring 220 °C and smaller (~ 5 nm) diameter microfibrils from wood requiring 180 °C for complete exchange to occur in 1 h.⁶⁹

There are many experimental results on the thermal response of cellulose from 25 to 300 °C, such as from calorimetry, thermogravimetry, and dielectric spectroscopy, which are difficult to assign to specific structural changes.^{70–72} Taken as a whole, these experimental results indicate that there are several changes in cellulose structure and heat capacity in this temperature range, which are also a function of microfibril size. These data suggest there are changes in layer spacing and hydrogen bond patterns, but molecular level details of the high-temperature phase have not been determined.

Simulations of Cellulose Structure. Starting from the recently solved high-resolution crystal structures, there has been a significant increase in the number of computational studies that probe cellulose structure and behavior, including at high temperature. The conformations of cellobiose and cellulose oligomers in water as a function of temperature were studied with replica exchange molecular dynamics by Shen and co-workers.⁴⁰ In previous molecular simulations of cellulose I β at high

temperature, a structural transition was observed with the Gromos 45a4 force field for infinite crystals, where there is no possibility of microfibril twist due to enforced periodic symmetry.⁷³ This study showed that during the 10 ns simulations the lattice angles changed as a function of temperature, and that the primary alcohol conformations exhibited an uneven and unexplained distribution along the crystal. Yui et al. simulated hydrated cellulose minicrystals with the GLYCAM04_L force field, and mentioned briefly that a structural change occurs at elevated temperatures, but structural details were not reported.⁵³ Mazeau reported microheterogeneity in cellulose I β hydrogen bond patterns, including the presence of interlayer hydrogen bonds at room temperature, in a simulation using the PCFF force field.⁷⁴ Lastly, hydrogen bonding in cellulose I β as a function of temperature has been studied with a lattice model, which explicitly described interchain and intrachain hydrogen bonds.⁷⁵ Shen and Gnanakaran demonstrated frustration and plasticity in hydrogen bonding networks with a computationally efficient model. A review of cellulose molecular dynamics simulations was recently published by Bellesia et al.⁷⁶

Here, we build on this previous body of computational work by examining the molecular-level details of the behavior of cellulose I β at high temperature with a hydrated 36-chain cellulose I β microfibril. Simulations were conducted with two modern atomistic force fields.^{77–79} Despite some differences in structure and dynamics at 227 °C (500 K) with these force fields, a common behavior emerges. We will report room temperature behavior of these and other carbohydrate force fields in a companion study.

From the simulation results presented here, we predict structural features of the high-temperature phase of cellulose I. Hydrogen bond patterns deviate significantly from the previously reported cellulose I β crystal structure, due to chain tilt and the presence of hydroxymethyl groups in the GG and GT conformations, but there are similarities to cellulose II and III_I conformations. Our results suggest possible explanations for several experimental observations from the literature including aggregation of cellulose microfibrils by thermal treatment, and H/D exchange as a function of temperature across microfibril crystal sizes, and the irreversible transformation of cellulose I α to I β . We propose several experimental approaches to probe this behavior for validation of the simulation predictions.

METHODS

We conducted MD simulations with two force fields for carbohydrates: GLYCAM06⁷⁷ and the most recent CHARMM carbohydrate force field, denoted C35.^{78,79} The MD simulations were conducted with the AMBER PMEMD program.⁸⁰ The CHAMBER program was used to convert input files for the CHARMM force field into a form compatible for use in PMEMD, and agreement of single-point energies and forces from PMEMD were validated by comparison to energies and forces output from CHARMM.^{81,82} The modified TIP3P model was used for water.^{83,84} Molecular graphics were generated with VMD.⁸⁵

The initial cellulose microfibril coordinates used in this study were constructed from the cellulose I β crystal structure.³ The microfibrils have a degree of polymerization of 40 (DP 40), with the cross section as the “diagonal” 36-chain model used in our previous work,⁵¹ which is suggested by lattice imaging of flax microfibrils.⁸⁶ The cellulose was solvated with a box of water

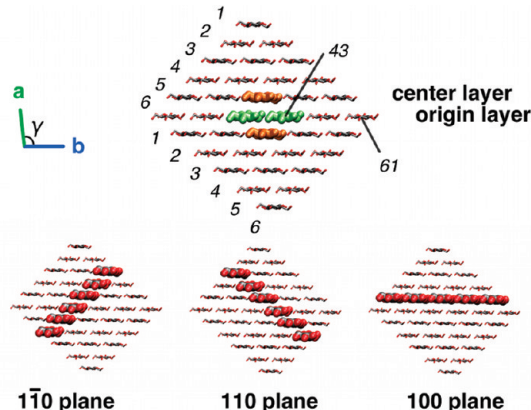


Figure 4. Initial 36-chain microfibril model of cellulose I β viewed down the chain axis from the nonreducing end, with the unit cell axes indicated at left. Chains are numbered on a 6×6 grid from 11 to 66. Chains 33, 34, and 43 are highlighted in orange (center chains) and green (origin chains). Lattice planes are indicated in the bottom images, arranged from left to right in order of widest to narrowest layer spacing between neighboring planes. The solvating water box and hydrogen atoms are not shown.

molecules equilibrated at 300 K and 1 atm with dimensions of 60 Å by 60 Å by 233 Å, which surrounded the cellulose with approximately 15 Å of water in each direction. The particle-mesh Ewald algorithm was applied for long-range electrostatics with a fft grid spacing of approximately 1 Å and κ of 0.275.⁸⁷ A scaling factor of unity was used for 1,4 nonbonded interactions. A cutoff distance of 10 Å was used for nonbonded interactions and a heuristic update was used to rebuild the nonbond list. The system was first minimized for 100 steps, then heated with the cellulose fixed from 0 to 500 K over 500 ps in increments of 50 K. The systems were further equilibrated at 500 K for 5 ns, and NVT production simulations were run for 100 ns, with a time step of 2 fs. Temperature was regulated with Langevin dynamics using a collision frequency of 1 ps^{-1} .⁸⁸ The SHAKE algorithm was used to constrain bond lengths involving hydrogen atoms,⁸⁹ and no conformational restraints were used during the production run.

We measured multiple order parameters to characterize the behavior of the cellulose microfibrils at high temperature for these force fields. The order parameters include overall twist of the microfibril, primary alcohol conformation as a function of location in the crystal, unit cell parameters, and the hydrogen-bonding partners both in a given layer and between layers. Figure 4 shows the grid numbering system for labeling individual chains. To avoid edge effects, we measured order parameters for the most interior 20 glucose monomers of the chains, unless otherwise stated.

Primary Alcohol Conformation. We measured primary alcohol conformations on monomers from chains 33, 42, 34, and 43. Conformations are reported with the TG, GT, GG nomenclature and color-coding scheme as in Figure 1.

Unit Cell Parameters. We measured unit cell distances and angles using C1 carbons in chains 33, 42, 34, 43, and 32. At each step, values were averaged over 20 unit cells from the interior of the microfibril (ignoring ends), and then averaged over the last 10 ns of the simulations.

Hydrogen Bonds. We report hydrogen bonds present more than 1% of the time between four interior chains: 33 and 42 in a center layer, and 34 and 43 in an origin layer. All possible donors

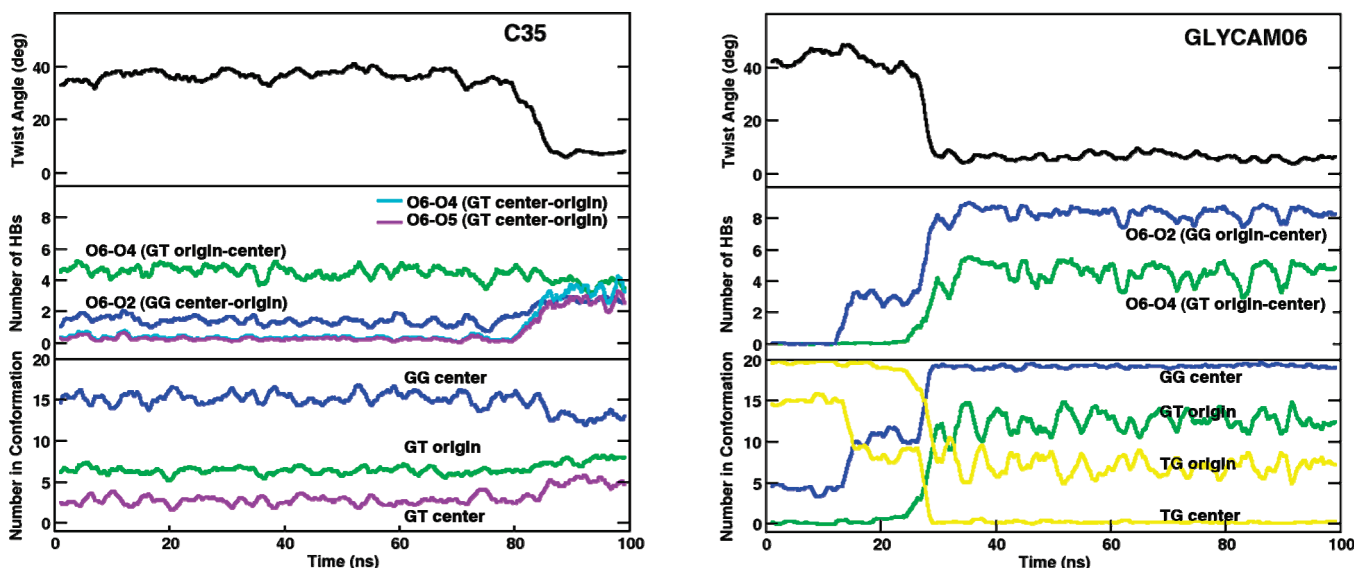


Figure 5. Microfibril twist as a function of time for the C35 and GLYCAM06 cellulose simulations (top panels). Relevant interlayer hydrogen bonds and primary alcohol conformations are also shown to indicate which structural changes are correlated with microfibril untwisting. Results are plotted as the moving average over a 200 ps window.

and acceptor pairs were included. The maximum distance for a hydrogen bond was defined as 3.5 Å between oxygen atoms, and O—H—O angle within 60° of linear. Three classes of hydrogen bonds are reported: intrachain, intralayer (between chains 33 and 42 or between chains 34 and 43), and interlayer. Interlayer hydrogen bonds are further divided as hydrogen bonds within 110 planes (between chains 33 and 43) or within $\bar{1}\bar{1}0$ planes (between chains 33 and 34). Hydrogen bonds between hydroxyl groups reported as oxygen pairs include both possible donor–acceptor pairings (i.e., O6—O2 includes both O6—HO6—O2 and O6—HO2—O2 hydrogen bonds). Hydrogen bonds to the ring oxygen O5 and the glycosidic oxygen O4 must have O5 or O4 as the acceptor.

Twist. We measured twist of the cellulose microfibrils as the dihedral angle between the four C1 atoms of the end monomers (1 and 40) of chains 25 and 52.

RESULTS

We report the behavior of hydrated DP 40, 36-chain cellulose I β microfibrils heated to 227 °C (500 K) for the C35 and GLYCAM06 force fields. Both the C35 and GLYCAM06 microfibrils twist during equilibration, and during the MD simulations the cellulose microfibrils untwist after a given induction time as shown in Figure 5. The C35 model untwists after an induction time of 80 ns and the untwisting event occurs over approximately 5 ns. The GLYCAM06 model untwists after 25 ns, and occurs in approximately 1 ns. To determine which structural changes occur simultaneously with the untwisting event, we also plot in Figure 5 the number of interlayer hydrogen bonds and the relevant primary alcohol conformation time series. There is a concurrent rise in the number of interlayer hydrogen bonds as the microfibril untwists for both simulations. In the C35 simulation, correlated with untwisting event, are transient bifurcated hydrogen bonds from center chains in the GT primary alcohol conformation to the glycosidic oxygen and ring oxygen in an origin layer, denoted as O6—O4 (GT center—origin) in light blue and O6—O5 (GT center—origin) in purple. The primary alcohol conformations

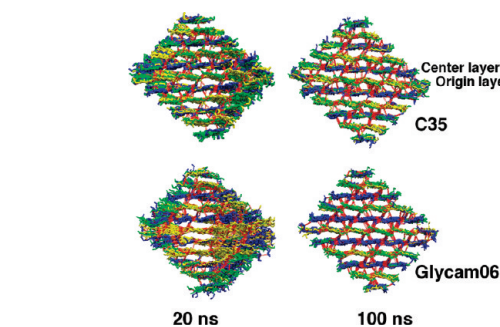


Figure 6. Snapshots of the simulations for the C35 and GLYCAM06 cellulose microfibril model before and after the untwisting event. Monomers are colored by primary alcohol conformation.

do not change substantially in the C35 simulation from the conformations adopted during equilibration, i.e. before $t = 0$, but there is a slight increase in the number of GT monomers in the center layers after the untwisting event. In the GLYCAM06 simulation, we observe a concurrent rise in the number of interlayer hydrogen bonds and the fraction of glucose monomers in the microfibril that are in the GG and GT conformations as the microfibril untwists. In the GLYCAM06 simulation, the increased number of O6—O2 (GG center—origin) interlayer hydrogen bonds and GG conformations are concurrent events, which occur in a two-stage transition during the untwisting of the microfibril. The O6—O4 hydrogen bonds occur when origin layer monomers adopt the GT conformation.

To visualize the untwisting transition, Figure 6 shows two snapshots of the central 20 monomers viewed from the non-reducing end of the microfibrils before ($t = 20$ ns) and after ($t = 100$ ns) the microfibrils untwist. Monomers are colored by primary alcohol conformation, and hydrogen bonds are shown as red lines. The C35 twisted microfibril exhibits some hydrogen bonds between the layers before the untwisting transition, with an increased number of interlayer hydrogen bonds after the transition. The GLYCAM06 simulation structure has few hydrogen

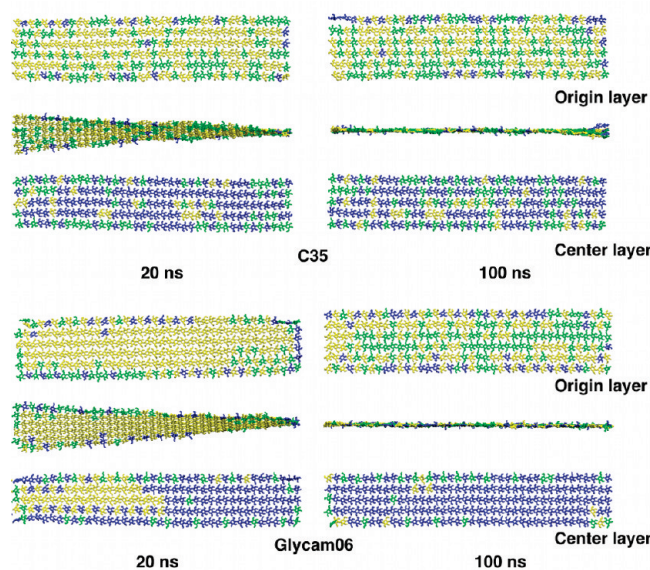


Figure 7. Center and origin layers for the C35 and GLYCAM06 cellulose microfibrils before and after the untwisting event. Monomers are colored by primary alcohol conformation. The top two views for each microfibril show an origin 100 layer shown from the face and from the side, and the third view is the center 100 layer labeled in Figure 6. A larger version of this figure is included in the Supporting Information.

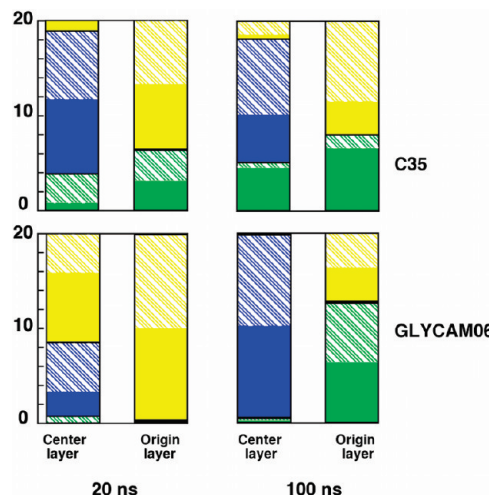


Figure 8. Average primary alcohol conformations for the C35 and GLYCAM06 simulations from 10 to 20 ns and 90 to 100 ns. Bars on the left are for center layers and the right bars are for origin layers. Primary alcohol conformations by color as in Figure 1, with TG on top, GG in the middle, and GT at the bottom. Hatched and solid colors represent even and odd residues, respectively, along single chains from the interior 20 monomers, 11 to 30 out of 40.

bonds between layers prior to the untwisting transition, and clearly exhibits a three-dimensional network at $t = 100$ ns. Despite differences between the two force fields, the structures after 100 ns are similar in terms of the three-dimensional hydrogen bond network, the overall untwisted shape, and the chain tilt in center and origin layers. Both simulation structures exhibit alternating mostly GG conformations in center layers, and both GT and TG conformation in origin layers.

Table 1. Lattice Parameters and d -Spacings from the High-Temperature Cellulose Simulations for C35, GLYCAM06, and X-ray Diffraction at High Temperature^a

	C35	GLYCAM06	230 °C ^b	280 °C ^b
$d_{1\bar{1}0}$ (nm)	0.616	0.613	0.609	0.614
d_{2110} (nm)	0.545	0.533	0.543	0.549
d_{3200} (nm)	0.400	0.398	0.400	0.411
a (Å)	8.06(0.07)	8.03(0.06)	8.06	8.23
b (Å)	8.40(0.07)	8.23(0.07)	8.26	8.21
c (Å)	10.42(0.02)	10.77(0.02)	10.37	10.37
α (deg)	93 or 87(1.1) ^c	90.1(1.0)	90.0	90.0
β (deg)	90.3(0.9)	90.0(0.7)	90.0	90.0
γ (deg)	97.1(0.9)	98.0(0.7)	96.6	96.4

^a Lattice parameter values from simulation are an average over the final 10 ns. Standard deviations are shown in parentheses. ^b From Wada et al.¹¹ ^c Ambiguously defined due to near $P2_1$ symmetry.

To visualize the spatial distribution of structural differences in center and origin layers, Figure 7 and Figure S5 (in the Supporting Information) show the individual chains in a center and origin layer for both force fields at $t = 20$ ns and $t = 100$ ns, with the reducing ends at left and nonreducing at ends right. The side views show the untwisting event, where the layers exhibit significant twist prior to the transition and are nearly flat after the transition. In the C35 simulation, there are more monomers with the GT conformation in the center layer after the transition. After the untwisting event, origin layers for C35 exhibits alternating TG/GT conformations along single chains, with neighboring glucose residues in the same TG/GT conformation across the chains in register (i.e., there are approximate vertical stripes of GT or TG). This alternating TG/GT pattern is accompanied by a small shift along the molecular axis between neighboring chains within a 100 layer, which will be discussed later in this section. In the GLYCAM06 simulation, origin layers change from nearly all TG, to a mixture of GT and TG. In the center layer, the transition from TG to the GG conformation proceeds from the nonreducing end and at $t = 20$ ns, approximately half of the center layer is in the GG conformation, which is shown quantitatively in Figure 5.

The average even/odd monomer spatial distributions of primary alcohol conformations along the length of the microfibrils are shown in Figure 8 as stacked bar charts. Table S1 in the Supporting Information shows these data in numerical form. As shown in Figure 8, the C35 simulation at $t = 100$ ns shows alternating conformations along the microfibril length, as indicated by unequal distribution of the hatched and solid fractions of the bars. In C35 origin chains, the TG and GT conformation start evenly distributed along the chain length, and after the untwisting transition, there is an unequal even/odd distribution. This indicates there is, on average over at least 10 ns, an alternating GT/TG pattern as shown for a single time step in Figure 7. In the GLYCAM06 simulation, center chains are almost completely GG. For origin chains, there is a transition from mostly TG conformation prior to the untwisting event to a combination of TG and GT after the microfibril untwists.

Lattice parameters of the high-temperature cellulose simulation structures are shown in Table 1 along with experimentally determined lattice parameters from the recent high-temperature fiber diffraction study from Wada and co-workers,¹¹ denoted

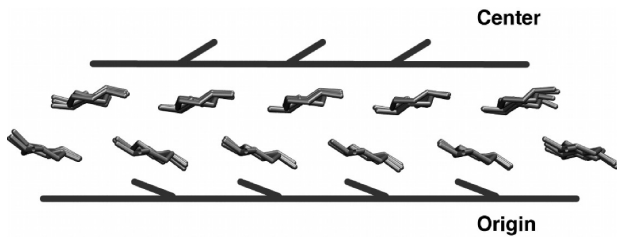


Figure 9. Chain tilt in a center and origin layer as viewed from the nonreducing end. This is an average structure over the final 10 ns of the GLYCAM06 simulation. Only carbon atoms are shown, with additional lines drawn to illustrate the opposite sense of chain rotation in origin and center chains.

I-HT. The sample material in this diffraction study was a nanocrystal film from *Cladophora* microfibrils, which were first annealed to form the I β polymorph. The lattice parameters for the C35 and GLYCAM06 models are quite similar overall, and reasonably similar to the I-HT experimental parameters. Time series of these lattice parameters are presented in Figure S1 in the Supporting Information. The main difference in unit cell for the C35 simulation structure is the α angle, which relates to relative displacement of chains within a hydrogen-bonded layer. During the untwisting event, the α angle of the C35 structure deviates from 90° by $\pm 3^\circ$. These two angles are indistinguishable due to the approximate $P2_1$ symmetry of the microfibril. A rotation of 180° about the microfibril axis reverses the sense of this angle, and it is expected that this angle may convert dynamically between the two complementary values if the alternating TG/GT pattern along single chains switches to the topologically equivalent GT/TG. This observation has significant potential implications for the diffraction patterns observed experimentally for high-temperature cellulose, which are discussed in the next section. For the GLYCAM06 model, the c lattice parameter (corresponding to the anhydrocellobiose repeat distance) is 0.4 Å larger than the experimental value, leading to a $\sim 4\%$ increase in microfibril length from the starting structure. This is a substantial difference, considering the presence of covalent bonds along this dimension.

Chains in each layer tilt, with center chains (mostly GG) tilting anticlockwise, and origin chains tilting clockwise as viewed from the nonreducing end (Figure 9). If the origin layers were entirely GT, the origin layers in these high-temperature simulation structures would be very similar in chain tilt and hydroxymethyl conformation to 110 layers in cellulose III $_I$. This alternating layer pattern of clockwise/anticlockwise chain tilt rotation may be important for the irreversible transformation of cellulose I α to I β .

Hydrogen bonds present in the initial I β room temperature structure are shown in Figure 10. Due to changes in hydroxymethyl orientation, many hydrogen bonds not present in the initial structure are formed at elevated temperature. We present hydrogen bonds in four categories, intrachain hydrogen bonds, intralayer hydrogen bonds between chains within a 100 plane, and interlayer hydrogen bonds between chains within 110 and 110 planes (Figures S2–S4 and Tables S2–S4 in the Supporting Information).

In the high temperature C35 and GLYCAM06 structures, intrachain O3–O5 hydrogen bonds are nearly fully occupied on average, but O6–O2 intrachain hydrogen bonds are only occasionally present (Table S2 in the Supporting Information).

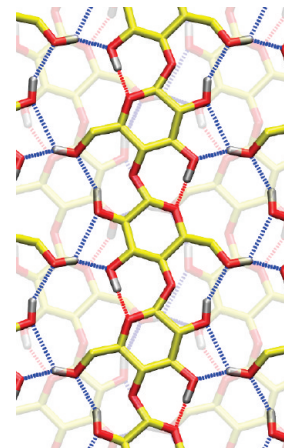


Figure 10. Hydrogen bonds in the initial cellulose I β room temperature structure. A center layer is in the foreground, with an origin layer in the background as viewed along the a -axis. Hydrogen bonds from O3 to O5 are in red, and other hydrogen bonds are in blue. Aliphatic hydrogen atoms are omitted.

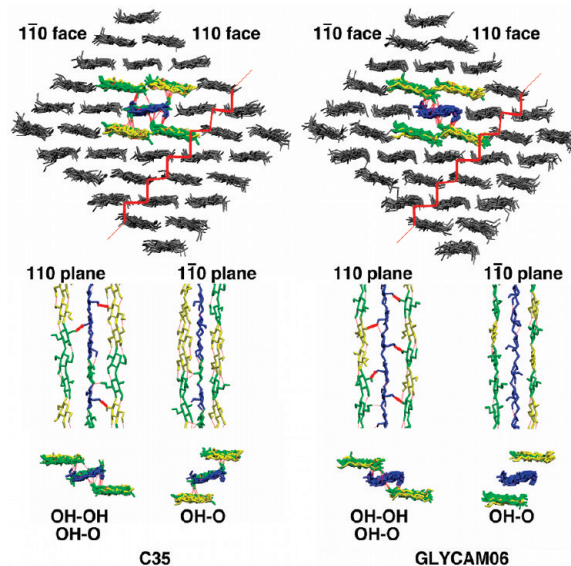


Figure 11. Interlayer hydrogen bonds. Microfibrils viewed from the nonreducing end (top and bottom), and from the sides (middle) for the C35 and GLYCAM06 structures at $t = 100$ ns. Hydrogen bonds within 100 planes are not indicated, but are present. The red lines indicate a proposed pathway for H/D exchange parallel to the 110 face. Aliphatic hydrogen atoms are omitted. A larger version of this figure is included in the Supporting Information.

This is largely due to the GT primary alcohol conformation in the high-temperature phase, for which O6–O2 intrachain hydrogen bonds are not possible (Figure 2).

Intralayer hydrogen bonds also differ from the initial patterns due to changes in hydroxymethyl orientation. The intralayer hydrogen bonds O2–HO2–O6 and O3–HO3–O6 are consistently more populated than intralayer O6–HO6–O2 and O6–HO6–O3 hydrogen bonds (Table S3 in the Supporting Information), as the O6 hydroxyl groups are also involved in interlayer hydrogen bonding.

We distinguish two categories of interlayer hydrogen bonds as either within 110 planes or within 110 planes (Figure S4 and

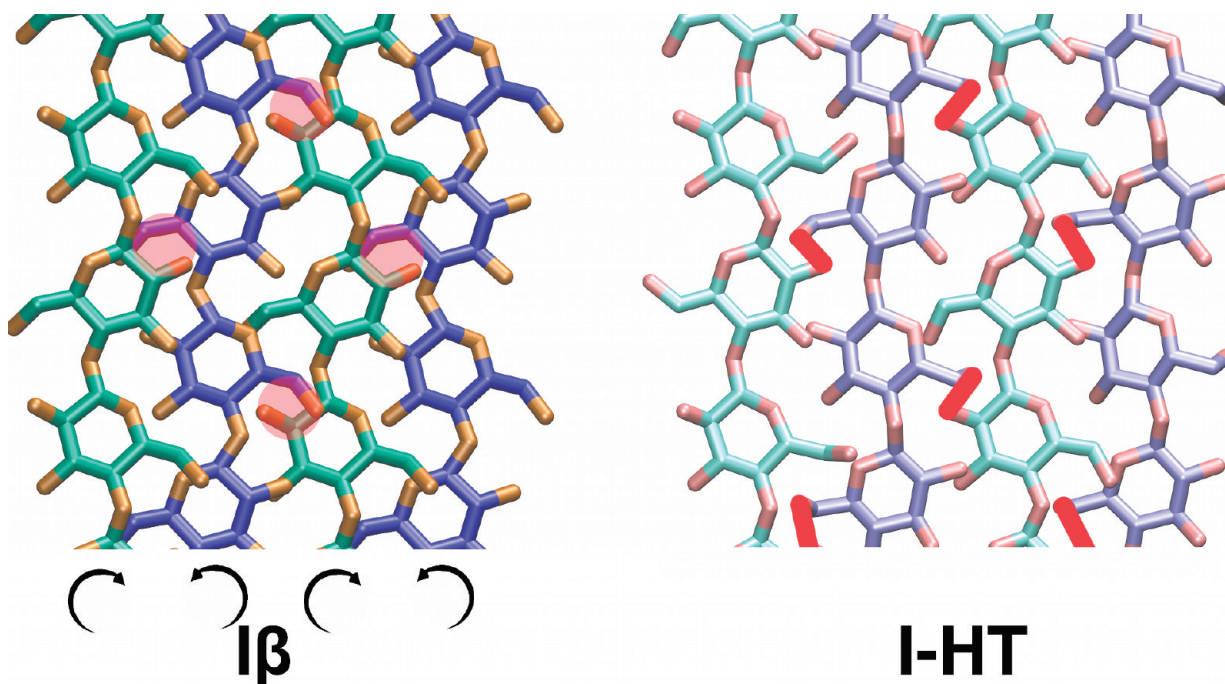


Figure 12. Four chains from a 110 plane of cellulose I β and the GLYCAM06 high-temperature structure. Red circles on the left indicate monomer pairs able to form interlayer O6–O2 hydrogen bonds at elevated temperatures, which are shown as red lines on the right. Center chains are blue and origin chains are green, corresponding to the hydroxymethyl conformations in the high-temperature structure. Curved arrows indicate the rotation sense of chain tilt as viewed along the chain axis with the nonreducing end near.

Table S4 in the Supporting Information). Hydrogen bonds within 110 planes are almost entirely between the O6 hydroxyl group and the glycosidic oxygen O4 or the ring oxygen O5. Hydrogen bonds within 110 planes include O6–O2 hydroxyl–hydroxyl hydrogen bonds, and some hydrogen bonds involving the glycosidic oxygen O4 or the ring oxygen O5. The presence of hydrogen bonds between hydroxyl groups along only one of these plane directions will affect the likely pathways for H/D exchange from the crystal surfaces, preferring a pathway parallel to 110 planes, as shown in Figure 11 with red lines.

The alternating pattern of center/origin layer hydroxymethyl conformations and chain tilt is due to the presence of hydrogen bonding between O6 in center chains to O2 in origin chains when the center chains are in the GG conformation. The P2₁ symmetry of these structures provides each monomer along each chain the same topology of neighbor interactions. Every monomer in center chains can make this interlayer hydrogen bond as shown in Figure 12. Successive monomers are rotated by 180° so chains in two origin layers within a 110 plane form these O6–O2 interlayer hydrogen bonds with a single center chain. This arrangement of interlayer hydrogen bonding and chain tilt would not be possible for cellulose I α -like layer packing, where there is P1 symmetry and only one chain per unit cell.

■ DISCUSSION AND CONCLUSIONS

We examined the high-temperature behavior of cellulose I β with two modern force fields. Both simulations predict structures that are not twisted, due to the formation of a three-dimensional hydrogen bond network different from the two-dimensional hydrogen-bonding network in the room temperature crystal structure of cellulose I β .³ This three-dimensional hydrogen bond network forms concurrently with the disappearance of twist. Both

models converge to a relatively similar high-temperature structure, despite differences in the C35 and GLYCAM06 force fields. The GLYCAM06 force field used here is nearly identical to the GLYCAM04_L force field used by Yui et al. in previous simulation studies of finite cellulose crystals, differing only in the C–O–C angle-bending parameter for the glycosidic linkage.^{52,53,90}

As described in previous reports, small-diameter finite cellulose crystals starting with the I β conformation twist due to the tendency of each individual chain to form a helical conformation, combined with frustration of this twist tendency by the presence of neighboring chains.⁵¹ There are no strong interactions between hydrogen-bonded layers in the initial structure, allowing the layers to slide relative to each other and form a twisted microfibril, similar to how β -sheets pack in proteins. Here we have shown that given sufficient simulation time the microfibrils untwist. In the C35 simulation, center chains adopt the GG during the equilibration period. The untwisting event in the C35 simulation is correlated with a small increase in interlayer hydrogen bonds as center-chain monomers rotate to the GT conformation. In the GLYCAM06 simulation, the untwisting event is correlated with an increased number of interlayer hydrogen bonds as center chain monomers adopt the GG conformation and origin chain monomers adopt the GT conformation. The long induction time (simulation time) required to observe these events casts doubt on the convergence of previous MD simulations of cellulose crystals, and it is also uncertain even if the present simulations have converged.

The results obtained in this study provide potential explanations for multiple sets of experimental data, including lateral aggregation of cellulose microfibrils during pretreatment and hydrolysis, H/D exchange experiments as a function of microfibril size, and high-temperature diffraction patterns. These data are discussed here in the context of our simulation study.

Implications of Untwisting Cellulose Microfibrils. This study demonstrates that changes in internal structure of cellulose microfibrils, through local interactions, can induce changes in cellulose structure at a large length scale. From our results, we hypothesize that untwisted cellulose microfibrils may have an impact in several experimentally observed phenomena, including enhanced microfibril aggregation as a function of heating or drying, periodic longitudinal disorder, and large-scale substrate movement during cellulase action on never-dried cellulose.

The average microfibril width in plant cell walls increases with hydrothermal treatment and extraction of noncellulosic components.^{91–94} If longitudinal segments of cellulose microfibrils untwist during thermal annealing and isolation, it is possible that this change enhances the cellulose aggregation propensity, thus leading to the experimental observation of lowered accessible surface area.^{95,96} However, because thermal treatment of the plant cell wall is a complex process involving multiple other biopolymers,^{97,98} the packing of cellulose bundles before and after thermal annealing remains an open, experimental question. Drying of plant cell walls also can induce changes in cellulose crystallites.^{99–101} Observations of an irreversible endothermic transition⁷⁰ and an irreversible change in dielectric absorption during the first heating to 50–140 °C⁷² indicate never-heated and never-dried cellulose may not have the same structure as cellulose which has been isolated through conventional methods. The metastable structure of native plant cellulose has been a hypothesis for many years.¹⁰²

Hydrogen/Deuterium exchange. As mentioned in the Background, it has been demonstrated that H/D exchange does not proceed to the interior of cellulose microfibrils at room temperature.⁶⁸ Depending on microfibril diameter, temperatures in the range 180–220 °C allow H/D exchange to cellulose microfibril interiors to occur. Interlayer spacing increases at elevated temperature, but complete H/D exchange can occur prior to the increase in layer spacing, given sufficient time and temperature (190 °C and 1.5 h⁶²). We assume the mechanism of hydrogen/deuterium exchange is by transfer between hydrogen-bonded hydroxyl groups as in water.¹⁰³ Water cannot penetrate between the chains of individual cellulose microfibrils, indicating it must be a change in the hydrogen bond network which allows for H/D exchange to proceed to the interior.

Our results indicate there are two dynamic H/D exchange pathways that can account for complete transfer to microfibril interiors. The two proposed H/D exchange pathways start either (1) from a microfibril end, proceeding along the length of the microfibril between two chains of a single 100 plane, or (2) in a zigzag pathway between chains in a 110 plane through O2–O6 or O6–O2 hydrogen bonds, across to a neighboring chain in a 100 plane, then again between chains in a 110 plane. This second proposed network is shown with red lines in Figure 10 and Figure S6 in the Supporting Information. We predict this second network will allow diffusion of H/D exchange effectively parallel to 110 surfaces but not parallel to 110 surfaces. Intermittent hydrogen bonds to O3 (Tables S3 and S4 in the Supporting Information) allow for complete H/D exchange within the microfibril interior. The interlayer hydrogen bonds present in the high-temperature phase reported here may form transiently at sufficiently high temperature⁷⁴ while still below the transition temperature for increased lattice spacing.

These results indicate that H/D exchange will not readily proceed between chains in 110 planes because there are almost no OH–OH hydrogen bonds in this direction. These proposed

anisotropic diffusion pathways could be tested experimentally by comparing H/D diffusion rates using rectangular cross section microfibrils with either larger 110 or 110 faces as substrates, and by using microfibrils of significantly different lengths. This experiment has been conducted in part using *Micrasterias crux-melitensis* rectangular Iβ ribbons, which has 20 nm 110 faces and 5 nm 110 faces.^{104,105} The *Micrasterias* ribbons achieve full H/D exchange similar to 5 nm diameter microfibrils,⁶⁹ which is consistent with our hypothesis of H/D exchange along a pathway parallel to 110 faces.

Diffraction Experiments of High-Temperature Cellulose. The most recent diffraction experiments on cellulose as a function of temperature by Wada and co-workers¹¹ used hydrothermally treated *Cladophora* cellulose, which natively has large diameter (~20–30 nm) Iα and Iβ crystals.¹⁰⁵ Hydrothermal treatment and limited sulfuric acid hydrolysis produced large diameter Iβ nanocrystals, which were aligned into oriented films. A recurring theme in diffraction studies of thermal expansion in cellulose is the anisotropic nature of the expansion, with smaller expansion coefficients along directions where hydrogen bonding is present.^{8–11,106} Thermal expansion coefficients from d-spacings along the Iβ phase 110, and 110 directions are equivalent and smaller than for the Iβ 100 direction, indicating little to no hydrogen bonding between layers for the Iβ phase. For the high-temperature phase, all three of these thermal expansion coefficients differ, with the 110 expansion coefficient larger than the 110 expansion coefficient, indicating more strong hydrogen-bonding interactions along 110 planes than along 110 planes,¹¹ which is consistent with the results presented in this study.

An unusual feature of the high-temperature diffraction patterns¹¹ is the presence of weak odd-order diffraction spots on the meridian (001 and 003), which should be disallowed if the space group is P2₁. Possible explanations for these weak odd-order spots suggested by these simulation structures include disorder in hydroxymethyl conformations, and disorder along the c direction, caused by a slight deviation in the α angle. There is no way to unambiguously assign the deviation in α as acute or obtuse within the frame of a hypothetical P2₁ unit cell. If the diffraction experimental results are due to the distribution over space or over time of the α angle value creating an average unit cell with α angle of 90°, this may be another explanation for the observed variation in intensity along the meridian.^{32,107}

The simulation results presented here can be validated via many experimental approaches to ascertain the structure of the predicted phase, either directly or indirectly. To our knowledge, the NMR spectrum of cellulose at high temperature has never been reported, although instruments exist which can operate at temperatures up to 250–300 °C.^{108,109} The NMR spectra of cellulose annealed at various temperature and pH conditions determined by Horii et al.^{110,111} illustrate the cellulose Iα to Iβ transformation, but they do not elucidate the structure of the high-temperature phase. Vibrational spectroscopy methods (IR⁶⁷ or Raman¹¹²) at high temperature may be able to determine changes in conformation beyond the currently reported changes in the hydroxyl-stretching region,^{65,66,113} if detectable changes occur when there is hydrogen bonding to the ring or glycosidic oxygen at high temperature, or if spectral changes due to rotation of the hydroxymethyl group can be detected,¹¹⁴ such as was done to detect changes in the Raman spectrum of cellulose due to treatment with NaOH.¹¹⁵ Scanning probe microscopy combined with tip-enhanced Raman spectroscopy may be able to detect conformational changes in single isolated microfibrils.¹¹⁶

Second-harmonic generation microscopy, which is sensitive to the electronic polarizability of a material, may be able to detect these proposed conformational changes at high temperature.^{117,118} Sum frequency generation is sensitive to conformations at interfaces,¹¹⁹ so this technique may be useful in following the surface to interior transformation of cellulose I α to I β .⁵⁷ It is expected that if heating cellulose fibrils causes long period twist to compress into short highly susceptible twisted sections, the leveling-off degree of polymerization may be sensitive to both the initial fibril diameter and to the severity (combined time and temperature) of the thermal treatment. To determine structural changes from the native state, experiments should be conducted on never-heated and never-dried cellulose microfibrils whenever possible, because traditional isolation methods may cause changes in microfibril structure and aggregation. From a simulation standpoint, to our knowledge, here we have conducted longer simulations of cellulose than have been reported to date. We note that the cellulose crystal shape used here is constructed from limited experimental data.⁸⁶ The results reported here are for structural changes in the interior of the crystal, and the actual temperature at which these changes occur will depend on crystal shape and size. We compared the high-temperature behavior of cellulose with two force fields, C35 and GLYCAM06. In these particular simulations, the structural behavior was relatively similar. We will examine the behavior of cellulose with these and other force fields at room temperature in a companion paper. While the simulations here are significantly longer than previously reported simulations of cellulose, it is not guaranteed the structures have converged. These results are qualitative predictions of the behavior of cellulose near 227 °C, and will not exactly match every experimental study at this temperature due to the crystal size and shape dependence previously discussed, as well as errors or approximations in the force fields.

We have used molecular simulation to determine structural features of the high-temperature phase of cellulose I, and we show that heating causes twisted cellulose microfibrils to untwist through the formation of a three-dimensional hydrogen bond network. The structural changes in these simulations suggest explanations for a broad range of experimental observations.

ASSOCIATED CONTENT

S Supporting Information. Four tables and six figures: lattice parameters as a function of time; average number of intrachain and intralayer hydrogen bonds; intrachain and intra-layer hydrogen bonds; and center and origin layers for the C35 and GLYCAM06 cellulose microfibrils. This material is available free of charge via the Internet at <http://pubs.acs.org>.

AUTHOR INFORMATION

Corresponding Author

*E-mail: James.Mathews@nrel.gov (J.F.M.); Michael.Crowley@nrel.gov (M.F.C.).

ACKNOWLEDGMENT

We thank the DOE Office of Science ASCR SciDAC program for funding. J.F.M., M.E.H., and M.F.C. were partially supported by the Center for Direct Catalytic Conversion of Biomass to Biofuels (C3Bio), an Energy Frontier Research Center funded by

the U.S. Department of Energy, Office of Science, Office of Basic Energy Sciences under Award No. DE-SC0000997. Computer time was provided by the TACC Ranger cluster under the National Science Foundation Teragrid grant no. MCB090159 and by the NREL Computational Sciences Center supported by the DOE Office of EERE under Contract no. DE-AC36-08GO28308. We thank Rajai Atalla, Vladimir Lulin, and Chris Pelkie for helpful discussions. M.B. thanks Alf de Ruvo Memorial Foundation of SCA AB and Sweden-America Foundation for financial support.

REFERENCES

- (1) Atalla, R.; Vanderhart, D. *Science* **1984**, 223, 283.
- (2) Sugiyama, J.; Persson, J.; Chanzy, H. *Macromolecules* **1991**, 24, 2461.
- (3) Nishiyama, Y.; Langan, P.; Chanzy, H. *J. Am. Chem. Soc.* **2002**, 124, 9074.
- (4) Nishiyama, Y.; Sugiyama, J.; Chanzy, H.; Langan, P. *J. Am. Chem. Soc.* **2003**, 125, 14300.
- (5) Langan, P.; Sukumar, N.; Nishiyama, Y.; Chanzy, H. *Cellulose* **2005**, 12, 551.
- (6) Nishiyama, Y.; Johnson, G. P.; French, A. D.; Forsyth, V. T.; Langan, P. *Biomacromolecules* **2008**, 9, 3133.
- (7) Kim, D.; Nishiyama, Y.; Wada, M.; Kuga, S.; Okano, T. *Holzforschung* **2001**, 55, 521.
- (8) Wada, M. *J. Polym. Sci., Polym. Phys.* **2002**, 40, 1095.
- (9) Hori, R.; Wada, M. *Cellulose* **2005**, 12, 479.
- (10) Hori, R.; Wada, M. *Cellulose* **2006**, 13, 281.
- (11) Wada, M.; Hori, R.; Kim, U.-J.; Sasaki, S. *Polym. Degrad. Stab.* **2010**, 95, 1330.
- (12) Atanassov, I. I.; Pittman, J. K.; Turner, S. R. *J. Biol. Chem.* **2009**, 284, 3833.
- (13) Tsekos, I. *J. Phycol.* **1999**, 35, 635.
- (14) Roberts, A.; Roberts, E. *Cellulose* **2004**, 11, 419.
- (15) Saxena, I. M. *Ann. Botany* **2005**, 96, 9.
- (16) Nishiyama, Y. *J. Wood Sci.* **2009**, 55, 241.
- (17) Gardner, K.; Blackwel., J. *J. Polym. Sci., Polym. Sym.* **1971**, 327.
- (18) Tucker, P.; George, W. *Polym. Eng. Sci.* **1972**, 12, 364.
- (19) Kennedy, C. J.; Cameron, G. J.; Sturcova, A.; Apperley, D. C.; Altaner, C.; Wess, T. J.; Jarvis, M. C. *Cellulose* **2007**, 14, 235.
- (20) Lahiji, R. R.; Xu, X.; Reifenberger, R.; Raman, A.; Rudie, A.; Moon, R. *J. Langmuir* **2010**, 100107082120075.
- (21) Niimura, H.; Yokoyama, T.; Kimura, S.; Matsumoto, Y.; Kuga, S. *Cellulose* **2010**, 17, 13.
- (22) Sturcova, A.; His, I.; Apperley, D.; Sugiyama, J.; Jarvis, M. *Biomacromolecules* **2004**, 5, 1333.
- (23) Ha, M.; Apperley, D.; Evans, B.; Huxham, M.; Jardine, W.; Vietor, R.; Reis, D.; Vian, B.; Jarvis, M. *Plant J.* **1998**, 16, 183.
- (24) Leppänen, K.; Andersson, S.; Torkkeli, M.; Knaapila, M.; Kotelnikova, N.; Serima, R. *Cellulose* **2009**, 16, 999.
- (25) Kim, U.-J.; Eom, S. H.; Wada, M. *Polym. Degrad. Stab.* **2010**, 95, 778.
- (26) Keller, A.; Hikosaka, M.; Rastogi, S.; Toda, A.; Barham, P.; Goldbeckwood, G. *Philos. Trans. R. Soc. A* **1994**, 348, 3.
- (27) Beckham, G. T.; Peters, B.; Starbuck, C.; Varianaval, N.; Trout, B. L. *J. Am. Chem. Soc.* **2007**, 129, 4714.
- (28) Beckham, G. T.; Peters, B.; Trout, B. L. *J. Phys. Chem. B* **2008**, 112, 7460.
- (29) Debzi, E.; Chanzy, H.; Sugiyama, J.; Tekely, P.; Excoffier, G. *Macromolecules* **1991**, 24, 6816.
- (30) Mosier, N.; Wyman, C.; Dale, B.; Elander, R.; Lee, Y.; Holtzapple, M.; Ladisch, M. *Bioresour. Technol.* **2005**, 96, 673.
- (31) Wada, M.; Chanzy, H.; Nishiyama, Y.; Langan, P. *Macromolecules* **2004**, 37, 8548.
- (32) Wada, M.; Heux, L.; Nishiyama, Y.; Langan, P. *Biomacromolecules* **2009**, 10, 302.

- (33) Biarnes, X.; Ardevol, A.; Planas, A.; Rovira, C.; Laiò, A.; Parrinello, M. *J. Am. Chem. Soc.* **2007**, *129*, 10686.
- (34) Zhu, Y.; Zajicek, J.; Serianni, A. *J. Org. Chem.* **2001**, *66*, 6244.
- (35) Barnett, C.; Naidoo, K. *J. Phys. Chem. B* **2008**, *112*, 15450.
- (36) Thibaudeau, C.; Stenutz, R.; Hertz, B.; Klepach, T.; Zhao, S.; Wu, Q.; Carmichael, I.; Serianni, A. *J. Am. Chem. Soc.* **2004**, *126*, 15668.
- (37) Woodcock, H. L.; Brooks, B. R.; Pastor, R. W. *J. Am. Chem. Soc.* **2008**, *130*, 6345.
- (38) Mason, P. E.; Neilson, G. W.; Enderby, J. E.; Saboungi, M.-L.; Cuello, G.; Brady, J. W. *J. Chem. Phys.* **2006**, *125*, 224505.
- (39) Stenger, J.; Cowman, M.; Eggers, F.; Eyring, E.; Kaatze, U.; Petracci, S. *J. Phys. Chem. B* **2000**, *104*, 4782.
- (40) Shen, T.; Langan, P.; French, A. D.; Johnson, G. P.; Gnanakaran, S. *J. Am. Chem. Soc.* **2009**, *131*, 14786.
- (41) Larsson, E. A.; Staaf, M.; Söderman, P.; Höög, C.; Widmalm, G. *J. Phys. Chem. A* **2004**, *108*, 3932.
- (42) French, A.; Johnson, G. *Cellulose* **2004**, *11*, 5.
- (43) Zhang, W.; Zhao, H.; Carmichael, I.; Serianni, A. S. *Carbohydr. Res.* **2009**, *344*, 1582.
- (44) Tang, H.; Belton, P. *Solid State Nucl. Magn. Reson.* **2002**, *21*, 117.
- (45) Kratochvil, P.; Suter, U. *Pure Appl. Chem.* **1989**, *61*, 211.
- (46) Corradini, P.; Auriemma, F.; De Rosa, C. *Acc. Chem. Res.* **2006**, *39*, 314.
- (47) Elazzouzi-Hafraoui, S.; Nishiyama, Y.; Putaux, J.-L.; Heux, L.; Dubreuil, F.; Rochas, C. *Biomacromolecules* **2008**, *9*, 57.
- (48) Xu, P.; Donaldson, L. A.; Gergely, Z. R.; Staehelin, L. A. *Wood Sci. Technol.* **2007**, *41*, 101.
- (49) Santa-Maria, M.; Jeoh, T. *Biomacromolecules* **2010**, *11*, 2000.
- (50) Hanley, S.; Revol, J.; Godbout, L.; Gray, D. *Cellulose* **1997**, *4*, 209.
- (51) Matthews, J.; Skopec, C.; Mason, P.; Zuccato, P.; Torget, R.; Sugiyama, J.; Himmel, M.; Brady, J. *Carbohydr. Res.* **2006**, *341*, 138.
- (52) Yui, T.; Hayashi, S. *Biomacromolecules* **2007**, *8*, 817.
- (53) Yui, T.; Nishimura, S.; Akiba, S.; Hayashi, S. *Carbohydr. Res.* **2006**, *341*, 2521.
- (54) Wilson, P.; Martin, D. *Macromolecules* **1996**, *29*, 842.
- (55) Akahane, T.; Mochizuk, T. *J. Polym. Sci., Polym. Lett.* **1970**, *8*, 493.
- (56) Divakara, S.; Niranjana, A. R.; Somashekar, R. *Cellulose* **2009**, *16*, 1187.
- (57) Horikawa, Y.; Sugiyama, J. *Biomacromolecules* **2009**, *10*, 2235.
- (58) Ghafouri, R.; Bruinsma, R. *Phys. Rev. Lett.* **2005**, *94*, 4.
- (59) Argeri, M.; Barone, V.; De Lillo, S.; Lupo, G.; Sommacal, M. *Physica D* **2009**, *238*, 1031.
- (60) Argeri, M.; Barone, V.; De Lillo, S.; Lupo, G.; Sommacal, M. *Theor. Math. Phys.* **2009**, *159*, 698.
- (61) Sturcova, A.; Davies, G.; Eichhorn, S. *Biomacromolecules* **2005**, *6*, 1055.
- (62) Horikawa, Y.; Itoh, T.; Sugiyama, J. *Cellulose* **2006**, *13*, 309.
- (63) Chanzy, H.; Henrissat, B. *FEBS Lett.* **1985**, *184*, 285.
- (64) Rowland, S.; Roberts, E. *J. Polym. Sci. A1* **1972**, *10*, 2447.
- (65) Watanabe, A.; Morita, S.; Ozaki, Y. *Appl. Spectrosc.* **2006**, *60*, 611.
- (66) Watanabe, A.; Morita, S.; Ozaki, Y. *Biomacromolecules* **2007**, *8*, 2969.
- (67) Marechal, Y.; Chanzy, H. *J. Mol. Struct.* **2000**, *523*, 183.
- (68) Horikawa, Y.; Sugiyama, J. *Cellulose* **2008**, *15*, 419.
- (69) Horikawa, Y.; Clair, B.; Sugiyama, J. *Cellulose* **2008**, *8*.
- (70) Szczesniak, L.; Rachocki, A.; Tritsch-Goc, J. *Cellulose* **2008**, *15*, 445.
- (71) Picker, K.; Hoag, S. *J. Pharm. Sci.* **2002**, *91*, 342.
- (72) Baranov, A. I.; Anisimova, V. N.; Khripunov, A. K.; Baklagina, Y. G. *Ferroelectrics* **2003**, *286*, 141.
- (73) Bergenstrahl, M.; Berglund, L. A.; Mazeau, K. *J. Phys. Chem. B* **2007**, *111*, 9138.
- (74) Mazeau, K. *Cellulose* **2005**, *12*, 339.
- (75) Shen, T.; Gnanakaran, S. *Biophys. J.* **2009**, *96*, 3032.
- (76) Bellesia, G.; Asztalos, A.; Shen, T.; Langan, P.; Redondo, A.; Gnanakaran, S. *Acta Crystallogr., Sect. D* **2010**, *66*, 1184.
- (77) Kirschner, K.; Yonge, A. B.; Tschampel, S. M.; Gonzalez-Outeirino, J.; Daniels, C. R.; Foley, B. L.; Woods, R. *J. Comput. Chem.* **2008**, *29*, 622.
- (78) Guvench, O.; Greene, S. N.; Kamath, G.; Brady, J. W.; Venable, R. M.; Pastor, R. W.; Mackerell, A. D. *J. Comput. Chem.* **2008**, *29*, 2543.
- (79) Guvench, O.; Hatcher, E.; Venable, R. M.; Pastor, R. W.; Mackerell, A. D. *J. Chem. Theory Comput.* **2009**, *5*, 2353.
- (80) Case, D. A.; Cheatham, T. E.; Darden, T.; Gohlke, H.; Luo, R.; Merz, K. M.; Onufriev, A.; Simmerling, C.; Wang, B.; Woods, R. J. *J. Comput. Chem.* **2005**, *26*, 1668.
- (81) Brooks, B. R.; Brooks, C. L.; Mackerell, A. D.; Nilsson, L.; Petrella, R. J.; Roux, B.; Won, Y.; Archontis, G.; Bartels, C.; Boresch, S.; Caflisch, A.; Caves, L.; Cui, Q.; Dinner, A. R.; Feig, M.; Fischer, S.; Gao, J.; Hodoscek, M.; Imw, M.; Kuczera, K.; Lazaridis, T.; Ma, J.; Ovchinnikov, V.; Paci, E.; Pastor, R. W.; Post, C. B.; Pu, J. Z.; Schaefer, M.; Tidor, B.; Venable, R. M.; Woodcock, H. L.; Wu, X.; Yang, W.; York, D. M.; Karplus, M. *J. Comput. Chem.* **2009**, *30*, 1545.
- (82) Crowley, M. F.; Williamson, M. J.; Walker, R. C. *Int. J. Quantum Chem.* **2009**, *109*, 3767.
- (83) Jorgensen, W.; Chandrasekhar, J.; Madura, J.; Impey, R.; Klein, M. *J. Chem. Phys.* **1983**, *79*, 926.
- (84) Durell, S.; Brooks, B.; Ben-Naim, A. *J. Phys. Chem.* **1994**, *98*, 2198.
- (85) Humphrey, W.; Dalke, A.; Schulten, K. *J. Mol. Graphics* **1996**, *14*, 33.
- (86) Naslund, P.; Vuong, R.; Chanzy, H.; Jesior, J. *Text. Res. J.* **1988**, *58*, 414.
- (87) Darden, T.; York, D.; Pedersen, L. *J. Chem. Phys.* **1993**, *98*, 10089.
- (88) Izaguirre, J.; Catarello, D.; Wozniak, J.; Skeel, R. *J. Chem. Phys.* **2001**, *114*, 2090.
- (89) Ryckaert, J.; Ciccotti, G.; Berendsen, H. *J. Comput. Phys.* **1977**, *23*, 327.
- (90) Yui, T.; Hayashi, S. *Cellulose* **2009**, *16*, 151.
- (91) Thimm, J. C.; Burritt, D. J.; Ducker, W. A.; Melton, L. D. *J. Struct. Biol.* **2009**, *168*, 337.
- (92) Inagaki, T.; Siesler, H. W.; Mitsui, K.; Tsuchikawa, S. *Biomacromolecules* **2010**, *11*, 2300.
- (93) Pingali, S. V.; Urban, V. S.; Heller, W. T.; Mcgaughey, J.; O'neill, H.; Foston, M.; Myles, D. A.; Ragauskas, A.; Evans, B. R. *Biomacromolecules* **2010**, *11*, 2329.
- (94) Foston, M.; Ragauskas, A. *Biomass Bioenergy* **2010**, *34*, 1885.
- (95) Jeoh, T.; Ishizawa, C. I.; Davis, M. F.; Himmel, M. E.; Adney, W. S.; Johnson, D. K. *Biotechnol. Bioeng.* **2007**, *98*, 112.
- (96) Ishizawa, C. I.; Jeoh, T.; Adney, W. S.; Himmel, M. E.; Johnson, D. K.; Davis, M. F. *Cellulose* **2009**, *16*, 677.
- (97) Donohoe, B.; Decker, S.; Tucker, M.; Himmel, M.; Vinzant, T. *Biotechnol. Bioeng.* **2008**, *101*, 913.
- (98) Brunecky, R.; Vinzant, T.; Porter, S.; Donohoe, B.; Johnson, D.; Himmel, M. *Biotechnol. Bioeng.* **2009**, *102*, 1537.
- (99) Einfeldt, J.; Kwasniewski, A. *Cellulose* **2002**, *9*, 225.
- (100) Zabler, S.; Paris, O.; Burgert, I.; Fratzl, P. *J. Struct. Biol.* **2010**, *171*, 133.
- (101) Quievry, N.; Jacquet, N.; Sclavons, M.; Deroanne, C.; Paquot, M.; Devaux, J. *Polym. Degrad. Stab.* **2010**, *95*, 306.
- (102) Stockman, Ve. *Biopolymers* **1972**, *11*, 251.
- (103) Riccardi, D.; König, P.; Prat-Resina, X.; Yu, H.; Elstner, M.; Frauenheim, T.; Cui, Q. *J. Am. Chem. Soc.* **2006**, *128*, 16302.
- (104) Kim, N.; Herth, W.; Vuong, R.; Chanzy, H. *J. Struct. Biol.* **1996**, *117*, 195.
- (105) Koyama, M.; Sugiyama, J.; Itoh, T. *Cellulose* **1997**, *4*, 147.
- (106) Wada, M.; Kondo, T.; Okano, T. *Polym. J.* **2003**, *35*, 155.
- (107) Arnott, S.; Hukins, D. *J. Mol. Biol.* **1973**, *81*, 93.
- (108) Thakur, K.; Newmark, R.; Kuehn, N.; Gregar, T. *Macromolecules* **2003**, *36*, 719.

- (109) Hu, W.; Hagihara, H.; Miyoshi, T. *Macromolecules* **2007**, *40*, 3505.
- (110) Yamamoto, H.; Horii, F.; Odani, H. *Macromolecules* **1989**, *22*, 4130.
- (111) Horii, F.; Yamamoto, H.; Kitamaru, R.; Tanahashi, M.; Higuchi, T. *Macromolecules* **1987**, *20*, 2946.
- (112) Wiley, J.; Atalla, R. *Carbohydr. Res.* **1987**, *160*, 113.
- (113) Hinterstoisser, B.; Salmen, L. *Vib. Spectrosc.* **2000**, *22*, 111.
- (114) Åkerblom, M.; Hinterstoisser, B.; Salmen, L. *Carbohydr. Res.* **2004**, *339*, 569.
- (115) Eronen, P.; Österberg, M.; Jääskeläinen, A.-S. *Cellulose* **2008**, *12*.
- (116) Yarbrough, J. M.; Himmel, M. E.; Ding, S.-Y. *Biotechnol. Biofuels* **2009**, *2*, 17.
- (117) Brown, R.; Millard, A.; Campagnola, P. *Opt. Lett.* **2003**, *28*, 2207.
- (118) Zimmerley, M.; Younger, R.; Valenton, T.; Oertel, D.; Ward, J.; Potma, E. *J. Phys. Chem. B* **2010**, *507*.
- (119) Chen, Z.; Shen, Y.; Somorjai, G. *Annu. Rev. Phys. Chem.* **2002**, *53*, 437.